Proc. Natl. Acad. Sci. USA
Vol. 90, pp. 8722–8726, September 1993
Neurobiology

Modulation of early sensory processing in human auditory cortex during auditory selective attention

(event-related field/magnetoencephalography/event-related potential/magnetic resonance imaging/Heschl's gyrus)

MARTY G. WOLDORFF*†, CHRISTOPHER C. GALLEN‡, SCOTT A. HAMPSON‡§, STEVEN A. HILLYARD*, CHRISTO PANTEV‡§, DAVID SOBEL¶, AND FLOYD E. BLOOM‡

*Department of Neurosciences, 0608, University of California at San Diego, 9500 Gilman Drive, La Jolla, CA 92093-0608; and Departments of ‡Neuropharmacology and ¶Radiology, Research Institutes of Scripps Clinic, La Jolla, CA 92037

Contributed by Floyd E. Bloom, June 4, 1993

ABSTRACT **Neuromagnetic fields were recorded from human subjects as they listened selectively to sequences of rapidly presented tones in one ear while ignoring tones of a different pitch in the opposite ear. Tones in the attended ear evoked larger magnetic brain responses than did unattended tones in the latency ranges 20–50 msec and 80–130 msec poststimulus. Source localization techniques in conjunction with magnetic resonance imaging placed the neural generators of these early attention-sensitive brain responses in auditory cortex on the supratemporal plane. These data demonstrate that focused auditory attention in humans can selectively modulate sensory processing in auditory cortex beginning as early as 20 msec poststimulus, thereby providing strong evidence for an "early selection" mechanism of auditory attention that can regulate auditory input at or before the initial stages of cortical analysis.**

Selective attention improves the perception of high-priority stimuli in the environment at the expense of other, less relevant, stimuli. In the auditory modality, for example, a person can attend selectively to a particular speaker's voice while tuning out other, simultaneous, conversations (the so-called "cocktail party" phenomenon). Despite extensive research (1–3), many gaps remain in our understanding of the neural and psychological mechanisms that underlie auditory selective attention.

The neural mechanisms of selective attention can be investigated noninvasively in humans by recording the brain's event-related electrical potentials (ERPs) and/or event-related magnetic fields (ERFs). ERPs and ERFs are extracted from the scalp-recorded electroencephalogram (EEG) or its magnetic counterpart, the magnetoencephalogram (MEG), by computer averaging the time-locked brain activity elicited by repeated stimulus occurrences. The resultant ERP and ERF waveforms reflect with high temporal resolution the patterns of neuronal activity that are evoked by a stimulus. By analyzing changes in the ERPs and ERFs as a function of the direction of attention, inferences can be made about the timing, level of processing, and anatomical location of stimulus selection processes in the brain.

Previous studies have recorded ERPs in an experimental analog of the cocktail party situation, with sequences of tone randomly presented to the left and right ears while subjects selectively attended to the tones in one ear and ignored tones in the opposite ear (4–7). Under conditions of high auditory sensory load, attended-ear tones were found to elicit an enlarged negative ERP wave that peaked at around 100 msec poststimulus and overlapped closely in time the major sensory-evoked negative wave, N100. An earlier positive wave in the interval 20–50 msec (the P20–50) was also found to be enlarged with attention (6, 7).

These ERP results support the view that the flow of auditory sensory information can be altered by attention at a relatively early stage of processing. They do not specify, however, the brain structures in which this stimulus selection takes place. One approach to address this question is to study neuromagnetic recordings (ERFs), which offer an advantage over ERPs for localization of the anatomical sources of evoked brain activity in cortical sulci (e.g., auditory cortex on the supratemporal plane). This advantage is due to ERF recordings being selectively sensitive to activity from such sources and due to magnetic fields being less distorted by the skull (8, 9).

Several studies have applied source localization techniques to ERF recordings and concluded that at least part of the enhanced activity elicited by attended sounds in the N100 latency range arises from the vicinity of auditory cortex (10, 11). However, the precise anatomical source(s) of this attention effect have yet to be verified by superposition of calculated source coordinates onto magnetic resonance (MR) images of the subjects' brains.‖ Even less information is available regarding the neural generator(s) of the P20–50 ERP attention effect, as no magnetic counterpart of this very early ERP modulation has yet been reported.

In the current study, neuromagnetic and MR imaging techniques were combined to localize the neuroanatomical origins of the early effects of attention on tone-evoked brain activity. The results provide evidence that focused auditory attention exerts selective control over early sensory processing in the auditory cortical areas on the supratemporal plane beginning at 20 msec poststimulus.

METHODS

Selective auditory attention was studied using the same fast-rate dichotic listening paradigm that we have used previously in ERP studies (6, 7), with the ERP recordings now complemented by recordings of neuromagnetic fields (ERFs)

The publication costs of this article were defrayed in part by page charge payment. This article must therefore be hereby marked "*advertisement*" in accordance with 18 U.S.C. §1734 solely to indicate this fact.

Abbreviations: ERF, event-related magnetic field; ERP, event-related electrical potential; MEG, magnetoencephalography(-gram); ECD, equivalent current dipole; EEG, electroencephalogram.

†To whom reprint requests should be sent at present address: Research Imaging Center, University of Texas Health Science Center at San Antonio, 7703 Floyd Curl Drive, San Antonio, TX 78284-6240.

§Present address: Institute of Experimental Audiology, University of Munster, Kardinal-von-Galen-Ring 10, D-4400 Munster, Germany.

‖There is considerable evidence that at least some of the "exogenous" tone-evoked activity (i.e., *non-attention-related*) in the 30- to 150-msec latency range arises from neural generators in the vicinity of the auditory cortex on the supratemporal plane (12–15). Recent neuromagnetic studies have localized portions of this early sensory-evoked activity to the supratemporal-plane auditory cortex as visualized on subjects' MR scans (16–18).

from over the left hemisphere using a 37-channel magnetometer. Seven normal volunteer subjects (ages 22–36) were studied in a magnetically shielded chamber. Tone sequences were delivered through a sound-tube system and consisted of 1000-Hz tone pips to the left ear and 3150-Hz tone pips to the right ear, all of 14-msec duration with 5-msec rise and fall times. The left- and right-ear tones were presented in random order with interstimulus intervals ranging randomly between 125 and 325 msec. The subjects' task was to listen selectively to the tones in one ear and detect occasional (9% per ear), difficult-to-detect, "target" tones that were 12 decibels (dB) fainter than the 55-dBSL (sensation level) "standard" tones in that ear. All tones in the other ear were to be ignored. Ten runs each of attend-left and attend-right conditions, each 2 min long, were presented in counterbalanced order. Only responses evoked by the right-ear standard tones (i.e., contralateral to the recording sites) are presented in this report.

The recording probe apparatus (Biomagnetic Technologies, San Diego) contained 37 magnetic sensors that utilized superconducting quantum interference devices (SQUIDs). This sensor array, spanning a circular area of 125-mm diameter, was placed over the scalp overlying the left auditory cortex. A transceiver-based system was used to localize the position of the magnetic sensor array relative to the head and to construct a spatial reference frame for the MEG measurements with respect to a set of fiducial skull landmarks. Three channels of EEG were also recorded over the left hemisphere from the International 10–20 System sites Cz, C3, and T3, referred to the left earlobe. The recording bandpass was 0.1–200 Hz for the MEG and 0.05–250 Hz for the EEG. For each subject, averaged ERF and ERP waveforms were obtained separately for the attended and unattended standards and targets. Trials with artifacts (e.g., eye blinks) were rejected from the averages. One magnetic sensor with highly elevated noise levels was excluded from analysis.

To quantify the effects of attention on the M100, mean amplitudes were measured separately for attended and unattended ERF waveforms for each subject across a latency window (80–130 msec) centered over the grand-average M100 peak. These measured values were then entered into an analysis of variance (ANOVA). To quantify activity in the earlier middle-latency range, statistical analyses were also performed on the magnetic M50 wave. The analyses on this wave, which in this experiment began at about 20 msec and lasted until 55 msec, were analogous to those for the M100, but with the measurement window set at 28–46 msec.

Topographic maps of the ERF distributions were calculated for the M50 and M100 peaks under the different attention conditions, both for the individual subjects' ERFs and for the ERFs grand-averaged over all the subjects. For each of these surface field distributions, a best-fitting equivalent current dipole (ECD) was calculated in the MEG reference frame (i.e., with respect to the fiducial skull landmarks), using an algorithm based on least-squares approxi-

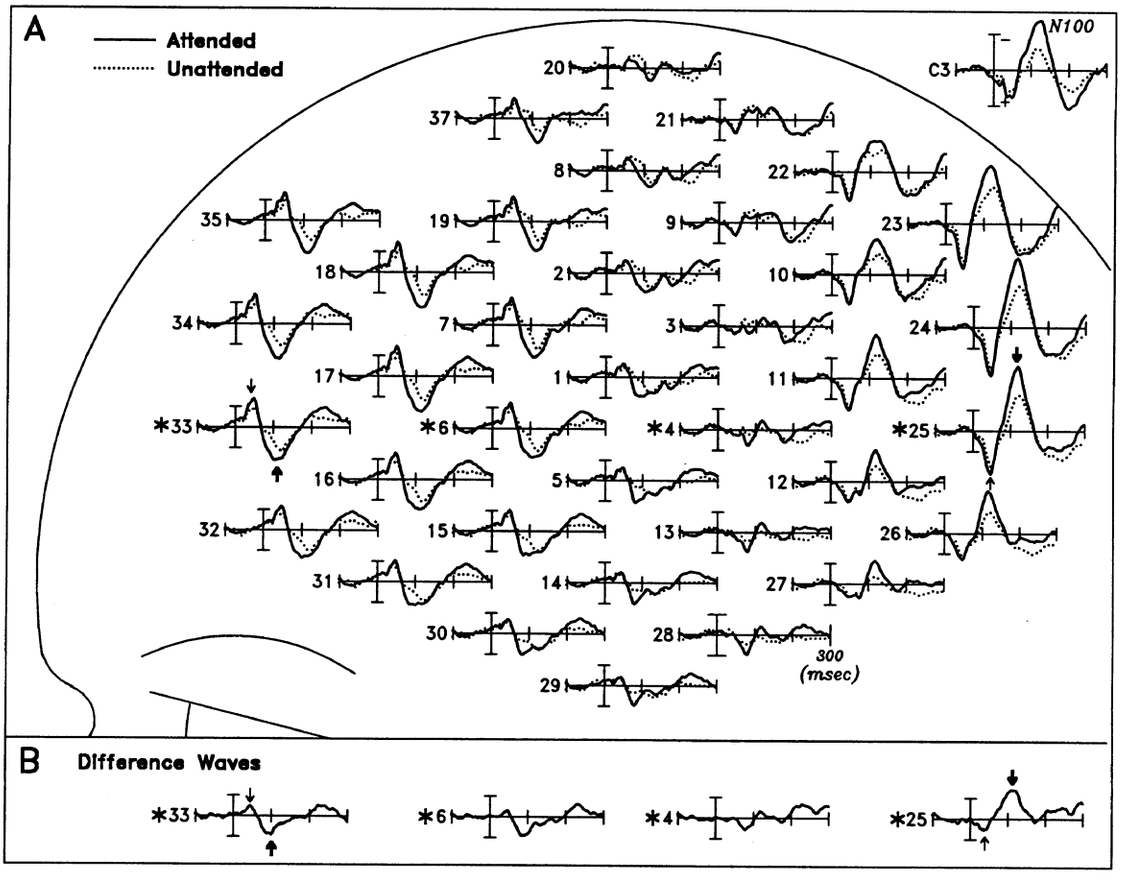

FIG. 1. (*A*) Grand-average waveforms (i.e., averaged across all seven subjects) of the event-related magnetic activity elicited by right-ear standard tones when they were attended versus when they were unattended, displayed at approximate locations of the magnetic sensors over the left hemisphere. At the upper right are the simultaneously recorded ERPs from the C3 site. Positive (upward) values for the magnetic activity indicate that the fields are directed out of the head, and negative values indicate inward-directed fields [calibration bars = ±20 femtotesla (fT)]. ERP scalp negativity is plotted upward [calibration bars = ±1 microvolt (μV)]. Large arrows mark the polarity-inverting M100 at sites 25 and 33; small arrows denote the polarity-inverting M50. (*B*) Grand-average attentional-difference waveforms (attended minus unattended ERFs) derived from the data in *A* for four sites (denoted with asterisks in *A*) in the anterior-to-posterior line across the array. Large and small arrows mark the polarity-inverting attention effects for M100 and M50, respectively.

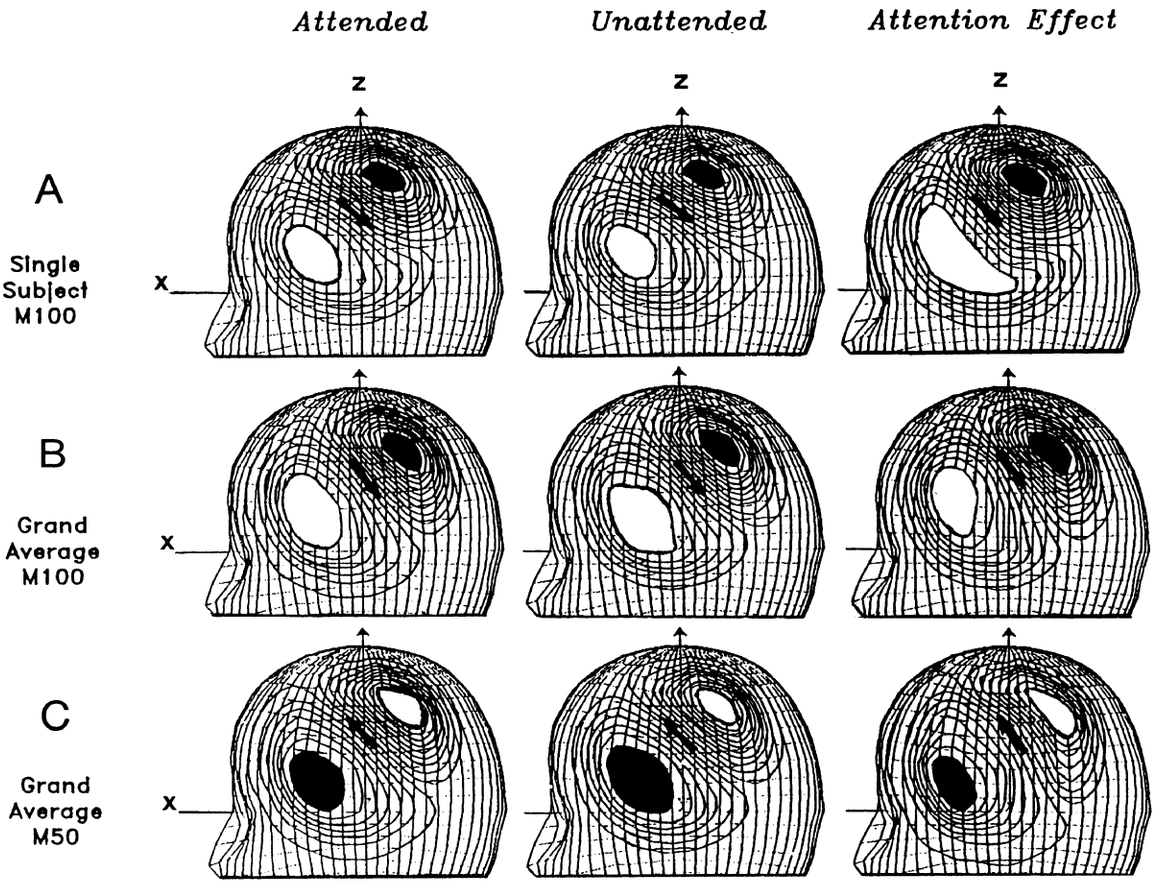

FIG. 2. Topographic plots (isocontour lines) showing magnetic field distributions for the M100 and the M50 (each individually scaled to emphasize distribution rather than absolute magnitude). (*A*) Field distributions at the peak of the M100 from a single subject for the attended response, the unattended response, and the attentional-difference wave (i.e., the subtracted difference between the attended and unattended responses). Note the dipolar field distribution, with a maximum (shaded dark) where the magnetic field lines are directed out of the head and a minimum (shaded light) where the magnetic field lines are directed into the head. The arrow indicates the direction of the single ECD source that would produce a set of fields that would best fit this distribution. Isocontour scales (differences between adjacent isocontour lines) are 12.4, 8.5, and 3.9 fT for the attended, unattended, and attentional-difference waves, respectively. (*B*) Corresponding field distributions for the M100 from the grand-averaged waveforms. Isocontour scales are 6.4, 3.7, and 2.9 fT for the attended, unattended, and attentional-difference waves, respectively. (*C*) Same as B for the M50. Isocontour scales are 4.8, 3.8, and 1.1 fT for the attended, unattended, and attentional-difference waves, respectively.

mation (19).** MR images were obtained for four of the subjects, and, using the skull landmarks, the neuromagnetic reference frames for these subjects were co-registered with their MR reference frames. This allowed these subjects' ECD localization coordinates to be transposed onto their MR images.

RESULTS AND DISCUSSION

A key feature of the paradigm used in this study is that it allows a comparison between the evoked responses to the same physical stimuli (e.g., right-ear standard tones) under different selective attention conditions (attend right ear versus attend left ear). Thus, any ERP or ERF differences found can be attributed to the internal focusing of attention either toward or away from those stimuli.

Fig. 1*A* shows the ERF and ERP waveforms for right-ear standard tones when they were attended versus unattended, grand-averaged across the seven subjects. As in previous studies (6, 7), attended-ear tones elicited an enhanced ERP negativity that closely overlapped the sensory-evoked N100 wave. A corresponding effect can also be seen on the magnetic counterpart to the N100, known as the M100 (e.g., see posterior channel 25). Moreover, both the M100 and its enhancement with attention exhibited a clear dipolar distribution—that is, the stimulus-evoked magnetic fields at 100 msec are directed out of the head posteriorly (e.g., channel 25, thick arrow) and into the head anteriorly (e.g., channel 33, thick arrow), with both of these extrema increasing in magnitude with attention.

The effect of attention on the amplitude of the M100 was reflected statistically in a significant ANOVA interaction of attention X site ($P < 0.008$, after applying the Huynh–Feldt correction for non-sphericity). This interaction was due to the M100 measures for the attended waveforms yielding larger positive values at posterior sites and larger negative values at anterior sites than for the corresponding unattended waveforms. In addition, specific comparisons at the extremum sites showed significantly larger magnitudes for the attended waveforms ($P < 0.006$–0.05).

The P20–50 ERP attention effect also was found to have a dipolar magnetic counterpart that we have termed the "M20–50" (Fig. 1*A*, channels 33 and 25, thin arrows). The M20–50 was evident as an augmentation of the magnetic M50 wave with attention. This effect was reflected statistically in a

**The ECD is the single equivalent dipole source that would produce a distribution of fields that would best fit an observed distribution. For the dipolar distributions analyzed in this report, the ECD location can be considered as representing the estimated centroid of the region of active tissue.

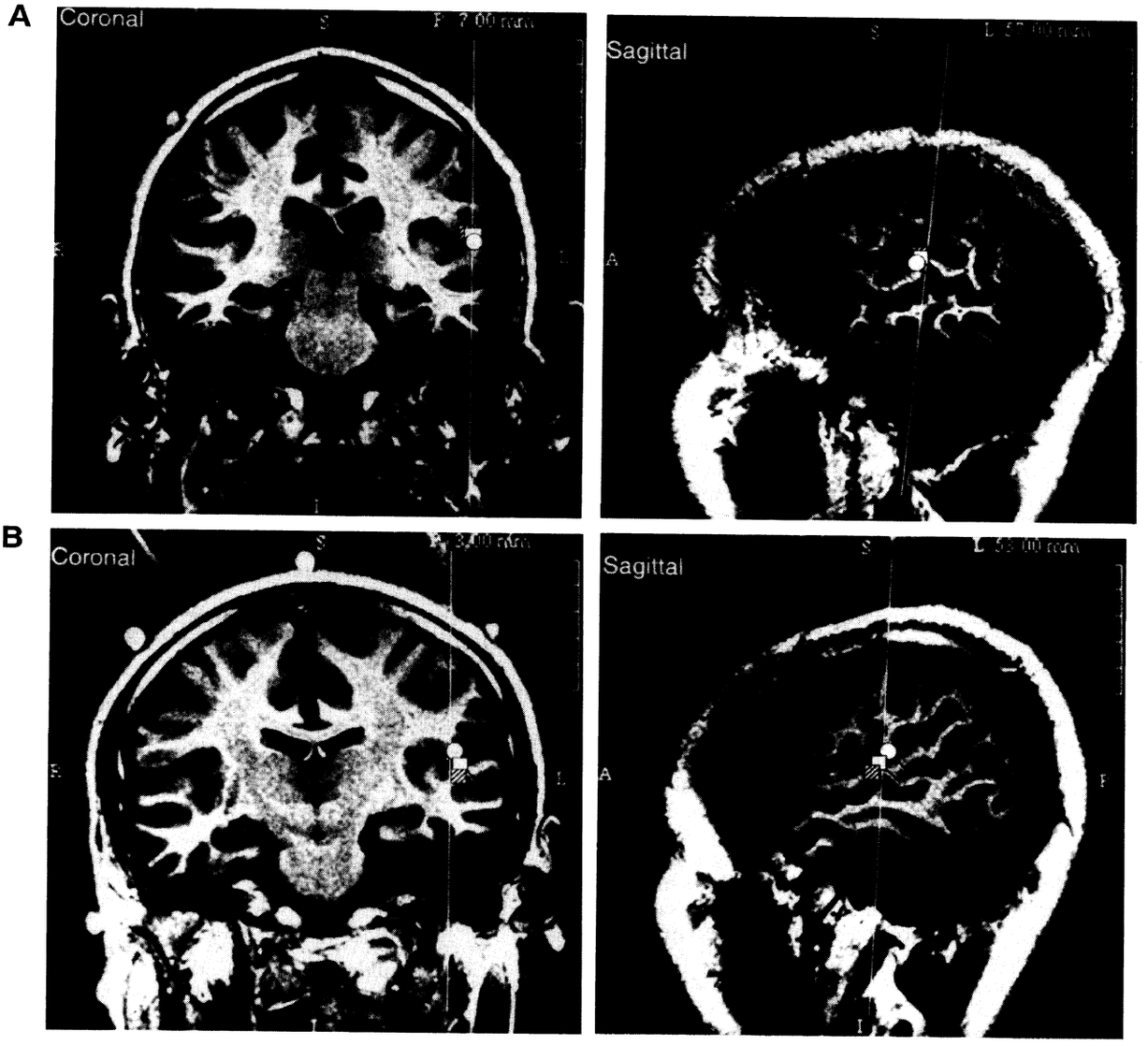

FIG. 3. (*A*) Coronal and sagittal MR images showing the estimated locations and angles of the ECD sources for the M100 and M100 attention effect for the subject whose ERF distributions are shown in Fig. 2*A*. The white square is for the attended M100, the hatched square is for the unattended M100, and the white circle is for the M100-latency attention effect. Note these estimated source locations are within millimeters of each other in auditory cortex on the supratemporal plane, localizing just lateral to Heschl's gyrus. The small black lines attached to each symbol indicate the direction of the estimated current dipole. The long vertical white line in each image indicates the plane through which the other image is taken. (*B*) Same as A for a second subject.

significant attention X site interaction in the M50 analysis ($P < 0.04$, after applying the Huynh–Feldt correction), which resulted from the ERF amplitude measures for the attended waveforms having larger positive values anteriorly and larger negative values posteriorly than for the unattended waveforms. Specific comparisons at the extremum sites also showed significantly larger magnitudes for the attended waveform M50s ($P < 0.025$–0.05).

The attention effects are highlighted in the "attentional-difference waves" formed by subtracting the unattended response waveform from its attended counterpart at each recording site. Fig. 1*B* shows these difference waves for four sites along an anterior-to-posterior line across the recording array through the M50 and M100 extrema. It can be seen that both the M20–50 attention effect (peaking at about 40 msec) and the M100-latency attention effect (peaking at 100 msec) invert at anterior sites relative to posterior sites in a manner similar to the M50 and M100 components themselves.

Topographic plots of the evoked magnetic field distributions at the peak of the M100 are shown in Fig. 2*A* for one of the subjects. Displayed are the ERF distributions of the M100 to attended tones, the M100 to unattended tones, and the attended-minus-unattended M100 attention effect. Each of these contour plots shows a highly dipolar distribution, with a single posterior maximum and single anterior minimum. This suggests that the activity in each case can be well modeled as arising predominantly from a focal dipolar source located a few centimeters deep (i.e., in the region of auditory cortex) and oriented parallel to the displayed arrow (i.e., perpendicular to the Sylvian fissure). The high degree of similarity among these three distributions suggests that their sources have similar locations and orientations.

For each subject, the best-fitting ECD was calculated in the MEG reference frame for each of these M100-latency surface field distributions. For most of the subjects, the observed field distributions for the M100 and for the M100-latency attention effect were each well accounted for by single ECDs, with correlations between the dipole model fields and the recorded fields ranging from 0.96 to 0.99. MR images were obtained for the four subjects with the best-fitting ECDs and

these subjects' ECD coordinates were transposed onto their MR images.

Fig. 3*A* shows a coronal and a sagittal MR section from one of these subjects and indicates the estimated locations and angles of the ECD sources for the attended M100, unattended M100, and M100-latency attention effect. These estimated source locations are indeed within millimeters of each other in auditory cortex on the supratemporal plane, localizing just lateral to Heschl's gyrus. In addition, the estimated direction of current flow in each case is oriented approximately perpendicular to the cortical surface of the supratemporal plane, as predicted by current dipole theory (8, 9). Estimated source locations for a second subject are shown in Fig. 3*B*, and again all three ECDs lie very near to Heschl's gyrus. The remaining two subjects for whom MR images were obtained showed similar patterns of ECD localization for the M100 and M100-latency attention effect. These MR localization results provide the strongest evidence to date that the magnetic attention effect at 100 msec arises predominantly from enhanced activity in supratemporal-plane auditory cortex and that this enhanced activity consists primarily of an attention-related modulation of the M100 neural generator.

The M20–50 attention effect had an insufficient signal/noise ratio in individual subjects to be successfully fit using the ECD source localization techniques. However, the consistency of the probe placements and magnetic responses across subjects allowed visualization of this effect in the grand average (Fig. 1). Fig. 2 *B* and *C* show the field distributions of the M100 and M50 derived from the grand-averaged attended, unattended, and attentional-difference waveforms. All six of these distributions were highly dipolar, suggesting that the relative location of the M20–50 source could be estimated by applying the ECD source localization approach to the grand-average data. Thus, best-fit ECDs were calculated for the grand-averaged distributions using averaged head-shape and probe-placement information. These calculations yielded excellent-fitting ECDs (correlations of 0.98–0.995) for each of the six grand-average M100 and M50 distributions shown in Fig. 2 *B* and *C*. Although these source estimates could not be localized directly on any individual subject's MR scan, their relative x–y–z coordinates in the MEG reference frame could be evaluated. In this frame, the grand-average M50 (to both attended and unattended tones) *and* the corresponding attention effect (i.e., the M20–50) were localized quite near (2–14 mm more medial) the grand-average M100s and the individual subjects' M100s. Because these M100 sources were localized in individual subjects to regions on the supratemporal plane in or slightly lateral to Heschl's gyrus, it follows that the earlier M20–50 attention effect also derives from this area.

The present study combined neuromagnetic and MR imaging techniques to demonstrate that focused auditory attention exerts a selective control over early sensory processing in the auditory cortex of the supratemporal plane. This cortical localization was verified by directly plotting the source coordinates for the attentional enhancement of the M100 component onto MR scans of the individual subjects' brains. In addition, the discovery of a still earlier magnetic attention effect (the M20–50) that arises from the same cortical area indicates that this selective control over sensory transmission can begin as early as 20 msec after stimulus onset. Furthermore, the waveshapes of these early attention effects took precisely the form of an amplitude modulation of the sensory-evoked cortical components M50 and M100. This result, coupled with the finding that the sources of these attention effects were co-localized with the sources of the corresponding sensory-evoked components, strongly suggests the existence of a mechanism of sensory gain control within the auditory input channels at or before the initial stages of cortical processing. Thus, these results not only add strong support for psychological theories of attention that posit an early, pre-perceptual selection of stimulus input, they also provide specific information concerning some of the neuroanatomical structures and physiological mechanisms by which such selection is accomplished.

We thank Jonathan C. Hansen and Paul Krewski for important technical assistance; Biomagnetic Technologies, Inc., for providing access to the magnetometer and associated facilities; and Steve Luck, Lourdes Anllo-Vento, Vince Clark, William Rogasner, Robert Hannah, and Helen Mayberg for useful comments on earlier versions of this manuscript. This work was supported by National Institute of Mental Health Grant MH-25594, Office of Naval Research Contract N00014-89-J-1743, National Institute of Neurological Disorders and Stroke Program Project Grant NS-17778, and the San Diego McDonnell–Pew Center for Cognitive Neuroscience. This is paper NP8170 from The Research Institutes of Scripps Clinic.

1. Kahnemann, D. & Treisman, A. (1984) in *Varieties of Attention*, eds., Parasuraman, R. & Davies, R. (Academic, London), pp. 29–61.
2. Hillyard, S. A. & Picton, T. W. (1987) in *Handbook of Physiology, Section 1, Vol. 5, Part 2*, ed. Mountcastle, V. B. (Am. Physiol. Soc., Baltimore), pp. 519–584.
3. Posner, M. & Petersen, S. (1990) *Annu. Rev. Neurosci.* **13,** 25–42.
4. Hillyard, S. A., Hink, R. F., Schwent, V. L. & Picton, T. W. (1973) *Science* **182,** 177–180.
5. Naatanen, R. (1990) *Behav. Brain Sci.* **13,** 201–288.
6. Woldorff, M. G., Hansen, J. C. & Hillyard, S. A. (1987) in *Current Trends in Event-Related Potential Research*, eds. Johnson, R., Rohrbaugh, J. W. & Parasuraman, R. (Elsevier, London), pp. 146–154.
7. Woldorff, M. G. & Hillyard, S. A. (1991) *Electroencephalogr. Clin. Neurophysiol.* **79,** 170–191.
8. Okada, Y., Lauritzen, M. & Nicholson, C. (1987) *Phys. Med. Biol.* **32,** 43–51.
9. Williamson, S. & Kaufman, L. (1987) in *Handbook of Electroencephalography and Clinical Neurophysiology: Methods of Analysis of Brain Electrical and Magnetic Signals*, eds. Gevins, A. & Remond, A. (Elsevier, New York), pp. 405–448.
10. Arthur, D., Hillyard, S. A., Flynn, E. & Schmidt, A. (1989) in *Advances in Biomagnetism*, eds. Williamson, S. J., Hoke, M., Stroink, G. & Kotani, M. (Plenum, New York), pp. 113–116.
11. Rif, J., Hari, R., Hamalainen, M. & Sams, M. (1991) *Electroencephalogr. Clin. Neurophysiol.* **79,** 464–472.
12. Romani, G. L., Williamson, S. J., Kaufman, L. & Brenner, D. (1982) *Exp. Brain Res.* **47,** 381–393.
13. Pelizzone, M., Hari, R., Makela, J., Huttunen, J., Alfors, S. & Hamalainen, M. S. (1987) *Neurosci. Lett.* **82,** 303–307.
14. Hari, R. & Lounasmaa, O. V. (1989) *Science* **244,** 432–436.
15. Scherg, M. & Von Cramon, D. (1986) *Electroencephalogr. Clin. Neurophysiol.* **65,** 344–360.
16. Yamamoto, T., Williamson, S. J., Kaufman, L., Nicholson, C. & Llinas, R. (1988) *Proc. Natl. Acad. Sci. USA* **85,** 8732–8736.
17. Pantev, C., Hoke, M., Lehnertz, K., Lutkenhoner, B., Fahrendorf, G. & Stober, U. (1990) *Electroencephalogr. Clin. Neurophysiol.* **75,** 173–184.
18. Arthur, D. L., Lewis, P. S., Medvick, P. A. & Flynn, E. R. (1991) *Electroencephalogr. Clin. Neurophysiol.* **78,** 348–359.
19. Marquardt, D. (1963) *SIAM J. Appl. Math.* **11,** 431–441.